International Journal of GEOMATE, April, 2025 Vol.28, Issue 128, pp.1-8
ISSN: 2186-2982 (P), 2186-2990 (O), Japan, DOI: https://doi.org/10.21660/2025.128.4859
Geotechnique, Construction Materials and Environment

ANALYTICAL SOLUTION FOR THE NONLINEAR BEHAVIOR OF STEEL-CONCRETE COMPOSITE GIRDERS

Hieu Nghia Hoang[1], *Quoc Anh Vu[2] and Manh Hien Nghiem[2]

[1]Department of Construction Engineering, Haiphong University, Vietnam; [2]Department of Civil Engineering, Hanoi Architectural University, Vietnam

*Corresponding Author, Received: 20 Dec. 2024, Revised: 23 Jan. 2025, Accepted: 26 Jan. 2025

ABSTRACT: This study proposes an analytical solution for the nonlinear inelastic analysis of statically determinate steel-concrete composite girders. The aim is to develop an exact method that accounts for key factors influencing nonlinear behavior, including gradual and distributed yielding. A novel approach for determining the moment-curvature curves of steel-concrete composite sections is introduced, offering significant reductions in computational time while improving accuracy compared to the fiber method. This solution addresses the lack of exact methods in the literature by presenting a highly accurate analytical approach that eliminates the need for subdividing girders into multiple elements or solving complex systems of equations, as required in numerical methods. Validation is achieved through comparisons of load-displacement curves with advanced numerical analyses and full-scale test results from the literature, demonstrating excellent agreement. These findings establish the proposed method as a reliable benchmark for validating numerical models and provide engineers with a straightforward yet precise tool for assessing deflection and material behavior in statically determinate girders.

Keywords: Steel – concrete composite girders, Nonlinear materials, Moment-curvature, Nonlinear analysis

1. INTRODUCTION

Many researchers have proposed advanced methods for the analysis, design, and construction of bridge girders to ensure their safety throughout their service life [1-3]. Steel-concrete composite structures are widely used in industrial, commercial, residential buildings, and bridges due to their inherent advantages, including high strength, excellent ductility, and ease of rapid fabrication and erection. However, linear elastic analysis cannot account for material and geometric nonlinearities, as well as imperfections such as residual stresses and initial geometric imperfections. When structural members approach their limit states, they typically exhibit an elasto-plastic response. Despite this, in limit state checks, the member forces are often derived from linear elastic analyses, which do not reflect real limit state conditions, leading to uncertainties in member reliability.

In the concentrated plastic hinge theory, plastic deformation is assumed to occur only at the two ends of an element. A plastic hinge forms once the bending moment exceeds the maximum elastic moment of the section, while regions outside the plastic hinges are assumed to remain elastic [4-7]. However, this approach is limited in accurately modeling flexural stiffness along the beam, as it depends on bending moment distribution. To improve accuracy, a single physical element may need to be subdivided into multiple smaller elements, which can result in significantly increased computational time.

In contrast, the distributed plasticity model allows the gradual spread of plasticity along the element. Two main approaches are typically used to model this behavior: (1) the displacement-based method (finite element approach) and (2) the force-based (flexibility) method. Deng and Ghosn [8] proposed a method to model the nonlinear behavior of bridge girders by evenly distributing the effects of nonlinearity over an equivalent grid element's plastic hinge length. In the displacement-based method [9], curvatures along the element are interpolated under the assumption of constant stiffness. While this approach achieves acceptable accuracy by using multiple elements per member, it becomes less efficient when stiffness changes due to material nonlinearity. On the other hand, the flexibility-based approach models gradual plasticity with only one element per physical member. However, its implementation in finite element programs is more complex [10]. Both approaches face challenges when assuming displacement functions, which are typically derived for prismatic sections [8-11]. When applied loads cause stress to exceed the elastic range, girders undergo gradual and distributed yielding, making prismatic section assumptions inadequate and reducing analysis accuracy.

To account for material nonlinearity, cross-sections are often discretized into fibers [6,7,10-14], where the uniaxial stress-strain relationship of each fiber models the material behavior. The moment-curvature relationship of the cross section is then developed based on this approach. The fiber method

is computationally intensive and can introduce errors in cases of highly nonlinear behavior or sharp transitions in material properties.

AASHTO/NSBA recommends both hand analysis and finite element methods for designing bridge girders [15]. However, in hand analysis, there is no explicit method for verifying service limit state control for permanent deflection, leaving engineers reliant on analysis software or numerical methods like the finite element method. While finite element solutions improve with higher mesh density or an increased number of elements, engineers must carefully select the mesh size, as too few elements can lead to significant errors in bridge analysis.

This study introduces a novel approach for developing an exact moment-curvature curve for steel-concrete composite cross-sections, offering a significant reduction in computational time and accuracy compared to the fiber method. Unlike previous research, which primarily benchmarked numerical methods against experimental data or other numerical approaches [6,7,10,11,14], this study addresses the absence of exact solutions in the literature by presenting a highly accurate analytical method. The proposed approach eliminates the need to subdivide girders into numerous elements or solve complex systems of equations, as required in numerical methods.

2. RESEARCH SIGNIFICANCE

This study introduces an innovative method to develop an exact moment-curvature curve for steel-concrete composite cross-sections, offering a breakthrough in accuracy and efficiency. Unlike the traditional fiber method, this approach drastically reduces computational time, making it highly practical for engineering applications. Furthermore, the research presents a precise solution for determining girder deflection, addressing a critical challenge in structural analysis. By improving the computational efficiency and accuracy of these calculations, this study contributes to the advancement of structural design methodologies, enabling engineers to optimize composite structures with greater precision and confidence. Its findings have broad implications for both academia and industry.

3. PROPOSED METHOD

3.1 Cross Section

The cross-section dimensions include concrete slab width (b_s) and thickness (t_s), steel I-section height (h), flange width (b_f), flange thickness (t_f), and web thickness (t_w), as shown in Fig. 1. The following assumption can be made: 1) a perfect bond between the steel and concrete components of a composite concrete-steel cross-section is assumed then after deformation, the plane section remains plane; 2) no shear and torsional interaction effects are accounted for in the steel and concrete constitutive models; and 3) large displacement and rotation but small strain.

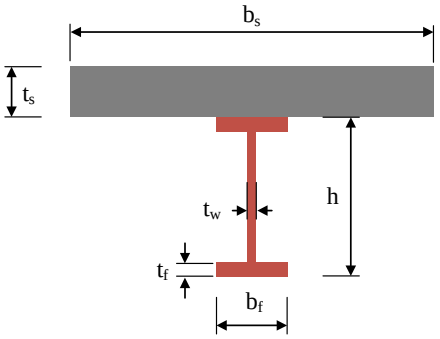

Fig. 1 Typical cross-section

3.2 The Behavior of Steel

The axial stress-strain relationship of steel material, both in tension and in compression, is assumed to be a multi-linear elastic-plastic [10], as shown in Fig. 2 and presented in Eq. (1) as follows:

$$\sigma_s = \begin{cases} \mathrm{s} E_s \varepsilon_s, \left|\varepsilon_s\right| \le \varepsilon_{ys} \\ \mathrm{s} f_{ys} + E_{hs1}\left(\varepsilon_s - \mathrm{s}\varepsilon_{ys}\right), \varepsilon_{ys} < \left|\varepsilon_s\right| \le \varepsilon_{hs} \\ \mathrm{s} f_{hs} + E_{hs2}\left(\varepsilon_s - \mathrm{s}\varepsilon_{hs}\right), \varepsilon_{hs} < \left|\varepsilon_s\right| \le \varepsilon_{us} \\ \mathrm{s} f_{us}, \varepsilon_{us} < \left|\varepsilon_s\right| \end{cases} \quad (1)$$

where ε_s is axial strain and σ_s is axial stress of the steel section; $s=s(\varepsilon_s)$ is signum function of ε_s, s=1 if $\varepsilon_s \ge 0$, and s=-1 if $\varepsilon_s<0$; ε_{ys}, ε_{hs}, ε_{us} denote yield, hardening and ultimate strains, respectively; E_s is Young's modulus; E_{hs1} and E_{hs2} are hardening moduli, represent the slopes of the yielding branches; f_{ys}, f_{hs}, and f_{us} are yield, hardening and ultimate strengths, respectively.

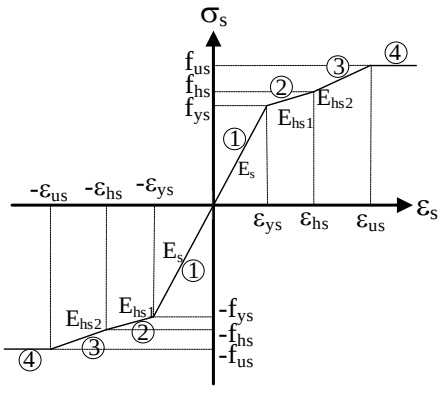

Fig. 2 The stress-strain relationship of steel

3.3 The Behavior of Concrete

Since concrete is used mostly in compression, the stress-strain relation in compression is of primary interest. The concrete stress-strain relation exhibits a nearly linear elastic response up to about 30% of the compressive strength then is followed by gradual hardening up to the concrete compressive strength when the material stiffness drops to zero. Beyond the compressive strength, the concrete stress-strain relation exhibits strain-softening until failure takes place by crushing. The monotonic envelope curve introduced by Kent and Park was adopted in this study for its simplicity and computational efficiency [16]. The monotonic stress-strain relation for concrete under compression is depicted in Eq. (2) as:

$$\sigma_c = \begin{cases} -f_c\left[2\left(\dfrac{-\varepsilon_c}{\varepsilon_{0c}}\right)-\left(\dfrac{\varepsilon_c}{\varepsilon_{0c}}\right)^2\right], -\varepsilon_{0c} \le \varepsilon_c \le 0 \\ -f_c\left[1-(1-\eta)\dfrac{-\varepsilon_c-\varepsilon_{0c}}{\varepsilon_{uc}-\varepsilon_{0c}}\right], -\varepsilon_{uc} \le \varepsilon_c < -\varepsilon_{0c} \\ -\eta f_c, \varepsilon_c < -\varepsilon_{uc} \end{cases} \quad (2)$$

where ε_c is axial strain and σ_c is axial stress of the concrete; f_c is prism compressive strength in uniaxial loading, taken as $0.76f_{uc}$, where f_{uc} represents the cubic compressive strength and can be approximately evaluated as $1.25f_{0c}$ where f_{0c} represents the cylinder compressive strength; E_c denoted Young's modulus of the concrete, can be computed by using ACI318-08 [17] equation as $E_c = 4700\sqrt{f_c(MPa)}$ (MPa) for normal weight concrete; ε_{0c} is a corresponding strain to f_c, $\varepsilon_{0c} = 2f_c/E_c$; ε_{uc} is ultimate strain; and η is residual stress factor.

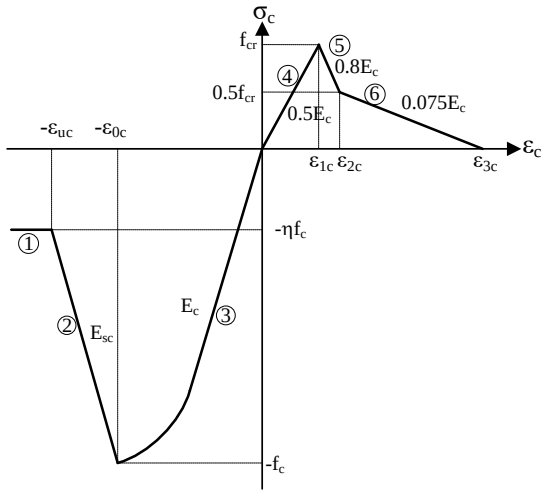

Fig. 3 The stress-strain relationship of concrete

The stress-strain relationship of concrete in tension developed by Vebo and Ghali [18] was adopted in this study, given in the following forms:

$$\sigma_c = \begin{cases} 0.5E_c\varepsilon_c, \varepsilon_c \le \varepsilon_{1c} \\ f_{cr} - E_{cr1}(\varepsilon_c - \varepsilon_{1c}), \varepsilon_{1c} < \varepsilon_c \le \varepsilon_{2c} \\ 0.5f_{cr} - E_{cr2}(\varepsilon_c - \varepsilon_{2c}), \varepsilon_{2c} < \varepsilon_c \le \varepsilon_{3c} \\ 0, \varepsilon_c > \varepsilon_{3c} \end{cases} \quad (3)$$

where f_{cr} represents the tensile strength of concrete; ε_{1c} is strain corresponding to cracking stress; ε_{2c} is strain corresponding to tensile stress reducing to half of cracking stress after cracking, $\varepsilon_{2c} = 2.625f_{cr}/E_c$; ε_{3c} is strain corresponding to zero tensile stress; and $E_{cr1}=0.8E_c$ and $E_{cr2}=0.075E_c$ are cracking moduli. The stress-strain curve of the concrete for both compression and tension is illustrated in Fig. 3. The number inside the circle indicates the segment number that is used to establish equation of stress to determine moment-curvature curve.

3.4 The Behavior of Steel Rebar

In the tensile region of concrete, the stress-strain relationship of an embedded rebar differs significantly from that of a bare bar due to the bond between the rebar and the surrounding cracked concrete. Upon the formation of cracks in the concrete, the stress on a steel bar decreases from its maximum value at the crack to its minimum at the midpoint between two adjacent cracks. When approaching yielding, the rebar at the crack typically yields first, while the one at the midpoint between two adjacent cracks remains under lower stress. This will result in nonuniform stress distribution along the rebar in the crack zone. Berlabi and Hsu proposed an average stress-strain curve to represent stress-strain relationship of the embedded rebar in tension [19], as shown in Fig. 4. This stress-strain curve can be expressed as the following equation:

$$\sigma_r = \begin{cases} E_r\varepsilon_r, -\varepsilon_{yr} \le \varepsilon_r \le \varepsilon_{nr} \\ f_{yr}\beta, \varepsilon_{nr} < \varepsilon_r \le \varepsilon_{ur} \\ f_{yr}, \varepsilon_r > \varepsilon_{ur} \\ -f_{yr}, \varepsilon_r < -\varepsilon_{yr} \end{cases} \quad (4)$$

Where ε_r is axial strain and σ_r is axial stress of the rebar; E_r and f_{yr} are Young's modulus and yield strength of the rebar material, respectively; f_{nr} and ε_{nr} is the average yield stress and yield strain, respectively; ε_{ur} is the ultimate strain; $B=(f_{cr}/f_{yr})^{1.5}/\rho$; ρ is longitudinal steel rebar ratio ($\rho \ge 0.25\%$); and $\beta=0.91-2B+(0.02+0.25B)\varepsilon_r/\varepsilon_{yr}$.

Berlabi and Hsu also proposed the average yield strain as [19]:

$$\varepsilon_{nr} = \varepsilon_{yr}(0.93-2B) \quad (5)$$

$$f_{nr} = E_r\varepsilon_{nr} \quad (6)$$

The ultimate strain can be derived from Eq. (4):

$$\varepsilon_{ur} = \varepsilon_{yr} \frac{0.09 + 2B}{0.02 + 0.25B} \quad (7)$$

The slope of the strain hardening branch of the rebar is obtained from derivation of Eq. (4) as:

$$E_{hr} = E_r \left(0.02 + 0.25B\right) \quad (8)$$

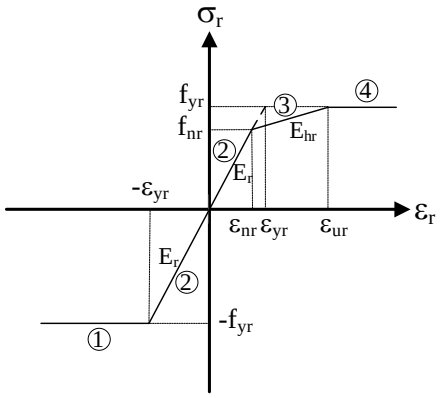

Fig. 4 The stress-strain relationship of rebar

3.5 Moment-Curvature Curve

Previously, most researchers utilized the fiber method to construct the moment-curvature curve [5-7,10,13,14]. A novel method for accurately obtaining this curve is described in this section [20].

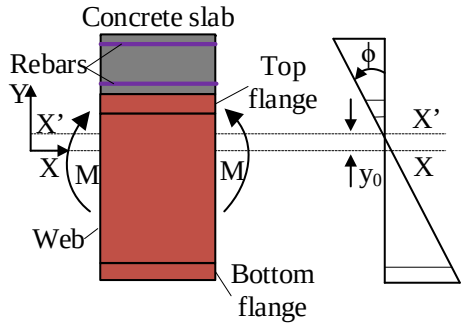

a) Strain distribution

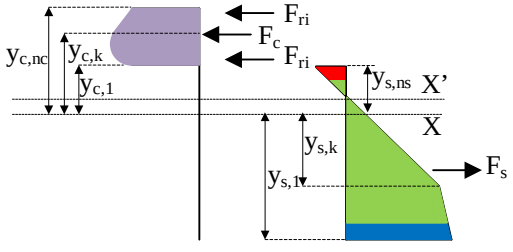

b) Stress distribution

Fig. 5 Strain and stress distributions

Figure 5a displays a portion of a steel-concrete composite girder with the cross-section depicted in Fig. 1. When subjected to a bending moment, M, curvature of the section is ϕ. The neutral axis shifts from X to X' upon loading with distance of two axes is y_0 to satisfy the equilibrium condition in the axial direction. The axial strain is assumed to be uniform horizontally and linearly varying vertically, as illustrated in Fig. 5a and determined as follows:

$$\begin{aligned} \varepsilon_c &= -\phi\left(y_c - y_0\right) \\ \varepsilon_s &= -\phi\left(y_s - y_0\right) \\ \varepsilon_r &= -\phi\left(y_r - y_0\right) \end{aligned} \quad (9)$$

where: ε_c, ε_s, and ε_r are axial strains in concrete slab, steel section, and rebar, respectively; y_c, y_s, and y_r are distances in the vertical direction (Y) from neutral axis X-X to the location that need to determine strains in concrete slab, steel section, and rebar, respectively, as shown in Fig. 5b. The stresses distributed along the cross section (Fig. 5b) are then derived from the stress-strain curves of concrete, steel section and rebar depending on the strain level (Figs. 2 to 4). Utilizing this stress distribution, the axial forces in the concrete slab (F_c), steel section (F_s) and rebars (F_r) can be formulated as:

$$\begin{aligned} F_c &= \sum_{k=1}^{n_c-1} b_s \int_{y_{c,k}}^{y_{c,k+1}} \sigma_{cj} dy_c \\ F_s &= \sum_{k=1}^{n_s-1} b \int_{y_{s,k}}^{y_{s,k+1}} \sigma_{sj} dy_s \\ F_r &= \sum_{i=1}^{n_r} F_{ri} = \sum_{i=1}^{n_r} A_{ri}\sigma_{rj} \end{aligned} \quad (10)$$

where: j is segment index on the stress-strain curves as displayed in circles shown in Figs. 2 to 4; A_{ri} is area of the i^{th} rebar; n_c and n_s are number of sub-ranges of concrete slab and steel section, respectively; n_r is number of the rebars; $b=b_f$ if sub-range is in the flange, and $b=t_w$ if sub-range is in the web; σ_{cj}, σ_{sj}, and σ_{rj} are stress functions of concrete slab, steel section and rebar, respectively, as presented in Table 1 to Table 3 by adopting Eqs. (1) to (4); k is index of boundaries of sub-ranges, defined by the boundaries of the concrete slab, the flange and web of the steel section, and any discontinuities on the stress-strain curves. By applying the corresponding strains at the boundaries of these sub-ranges to the stress-strain curves, the stress in each sub-range can be determined. Since no external axial force is applied to the girder, the resultant force of the cross-section should be zero as follows:

$$F_c + F_s + F_r = 0 \quad (11)$$

The distance y_0 between X and X' is determined iteratively. Initially, y_0 is set to zero and then adjusted to satisfy Eq. (11). Once Eq. (11) is satisfied, the bending moments are calculated as follows:

$$M = M_c + M_s + M_r \quad (12)$$

where M_c, M_s, and M_r are bending moments about neutral axis in concrete slab, steel section, and rebars, respectively and determined as follows:

$$M_c = \sum_{k=1}^{n_c-1} b_s \int_{y_{c,k}}^{y_{c,k+1}} \sigma_{cj} y_c dy_c$$

$$M_s = \sum_{k=1}^{n_s-1} b \int_{y_{c,k}}^{y_{s,k+1}} \sigma_{sj} y_s dy_s \quad (13)$$

$$M_r = \sum_{i=1}^{n_r} A_{ri} \sigma_{rj} y_{ri}$$

Table 1. Stress functions for concrete slab

j	σ_{cj}	Strain
1	$-\eta f_c$	$\varepsilon_c < -\varepsilon_{uc}$
2	$-f_c\left[1-(1-\eta)\frac{\phi(y_c-y_0)-\varepsilon_{0c}}{\varepsilon_{uc}-\varepsilon_{0c}}\right]$	$-\varepsilon_{uc} \le \varepsilon_c < -\varepsilon_{0c}$
3	$-f_c\left[2\phi\frac{(y_c-y_0)}{\varepsilon_{0c}}-\phi^2\left(\frac{y_c-y_0}{\varepsilon_{0c}}\right)^2\right]$	$-\varepsilon_{0c} \le \varepsilon_c \le 0$
4	$-0.5E_c\phi(y_c-y_0)$	$\varepsilon_c \le \varepsilon_{1c}$
5	$f_{cr}-E_{cr1}(-\phi y_c+\phi y_0-\varepsilon_{1c})$	$\varepsilon_{1c} < \varepsilon_c \le \varepsilon_{2c}$
6	$0.5f_{cr}-E_{cr2}(-\phi y_c+\phi y_0-\varepsilon_{2c})$	$\varepsilon_{2c} < \varepsilon_c \le \varepsilon_{3c}$

Table 2. Stress functions for steel section

j	σ_{sj}	Strain
1	$-sE_s\phi(y_s-y_0)$	$\lvert\varepsilon_s\rvert \le \varepsilon_{ys}$
2	$sf_{ys}-E_{hs1}[\phi(y_s-y_0)+s\varepsilon_{ys}]$	$\varepsilon_{ys} < \lvert\varepsilon_s\rvert \le \varepsilon_{hs}$
3	$s\,f_{hs}-E_{hs2}[\phi(y_s-y_0)+s\,\varepsilon_{hs}]$	$\varepsilon_{hs} < \lvert\varepsilon_s\rvert \le \varepsilon_{us}$
4	sf_{us}	$\varepsilon_{us} < \lvert\varepsilon_s\rvert$

Table 3. Stress functions for rebar

j	σ_{rj}	Strain
1	$-f_{yr}$	$\varepsilon_r < -\varepsilon_{yr}$
2	$-E_r\phi(y_r-y_0)$	$-\varepsilon_{yr} \le \varepsilon_r \le \varepsilon_{nr}$
3	$f_{nr}-E_{hr}\varepsilon_{nr}-E_{hr}\phi(y_r-y_0)$	$\varepsilon_{nr} < \varepsilon_r \le \varepsilon_{ur}$
4	f_{yr}	$\varepsilon_r > \varepsilon_{ur}$

3.6 Displacements of The Girders

Since these girders are statically determinate, the bending moment can be determined solely from equilibrium equations. Based on bending moments along the girder and moment-curvature curve, the curvature along the girder can be obtained as:

$$\phi = \phi(M) \quad (14)$$

The rotation and displacement of the girders can then be calculated based on the moment-curvature curve as follows:

$$\theta = \int \phi dx + C$$
$$w = \int\int \phi dx dx + Cx + D \quad (15)$$

where θ and w are rotation and displacement of the girder; C and D are constants of integrations determined from boundary conditions. Equation (15) can be implemented using the Riemann integral, which is defined as a limit of sums. This approach, as described by Bear [21], allows for the calculation of the integral by summing the contributions from each small segment of the girder and taking the limit as the segment size approaches zero.

4. EXAMPLES AND DISCUSSIONS

4.1 The Cantilever Beam

The accuracy of the proposed method for analyzing the steel-concrete composite beam was validated using the cantilever beam model of Ngo-Huu [5]. This beam comprised a W12x27 steel section and a concrete slab measuring 0.102 m x 1.219 m, illustrated in Fig. 6a.

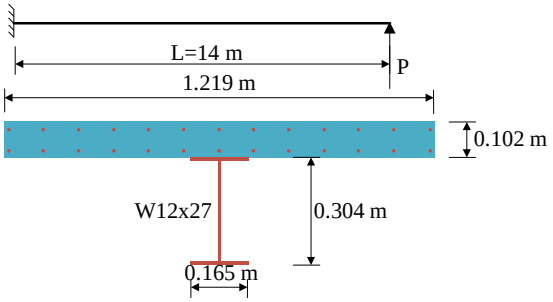

a) Geometry and cross section

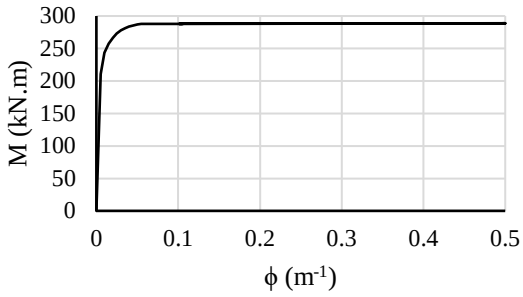

b) Developed moment-curvature curve

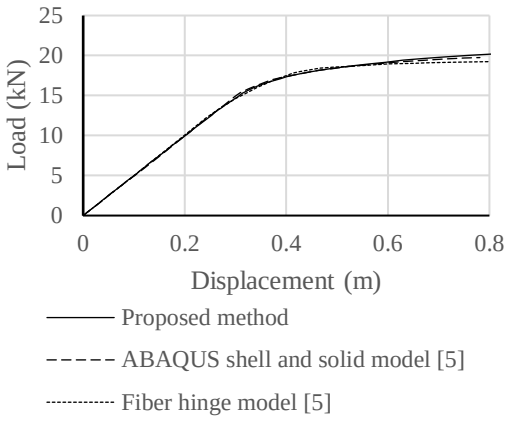

c) Load-displacement curves

Fig. 6. The cantilever steel-concrete composite beam

The compressive strength of the concrete slab was 16 MPa, from which the tensile strength f_{cr}=2.48 MPa, Young's modulus E_c=16016 MPa, and ε_{0c}=0.002 of the concrete slab were derived. The residual strength factor η was set to 1.00 to align with the concrete model used in Ngo-Huu [5]. The effect of the rebars were ignored in this analysis. The Young's modulus, yield strength and hardening modulus of structural steel were determined to be E_s=2x10^5 MPa. f_{sy}=252.4 MPa and E_{sh}=750 MPa, respectively.

Based on the section properties, the moment-curvature curve was developed, as shown in Fig. 6b. The proposed method was compared with the ABAQUS shell and solid models, as well as the fiber hinge model from Ngo-Huu [5], as illustrated in Fig. 6c. The results from the proposed method demonstrated excellent agreement with the ABAQUS shell and solid models. However, the fiber hinge model slightly underpredicted the results beyond the yield point. The proposed method, being analytical and simple, provides more accurate predictions compared to the plastic hinge model in this example.

4.2 The Simply Supported Girder

Two simply supported steel-concrete composite girders, SCB-1 and SCB-3, subjected to sagging moments were tested by Nie and Cai [22] and analyzed numerically using an advanced mixed finite-element approach by Nie et al. [23]. Additionally, Chiorean [10] analyzed the girders using a girder finite-element approach. The geometry, materials and section properties of the test girders are depicted in Figs. 7a and 8a. The cubic compressive strength of the concrete in compression is f_{cu}=27.7 MPa. The following properties were computed: f_c= 210.52 MPa, E_c=21564.76 MPa, f_{cr}=2.84 MPa, ε_{0c}=0.00195. The tensile strength of the concrete is considered according to the model described in Fig. 3. The behavior of the reinforced bars, both in tension and compression, are modelled according to the model described in Fig. 4 with the yield strength f_{yr}=290 MPa. The yield stress of the structural steel is f_{sy}=310 MPa, Young's modulus is E_s=20000MPa, E_{sh1}=0, and the strain hardening modulus is E_{sh2}=100 MPa, the corresponding strains are ε_{sy}=0.025, ε_{sh}=0.1, and ε_{su}=0.2.

The moment-curvature curves for the cross sections are illustrated in Figs. 7b and 8b, with maximum bending moments of approximately 210 kN.m and 250 kN.m for the SCB-1 and SCB-3 girders, respectively. These values are close to the maximum bending moments reported by Nie et al. [23]. The comparison of load-displacement curves between the proposed method, numerical methods and test results for SCB-1 girder is plotted in Fig. 7c. The proposed method matches perfectly the numerical methods but all of them slightly unpredicted the capacity of the girder. The maximum difference of the capacity is about 5 kN (3.8%) at the displacement of 0.04 m, considered an acceptable error.

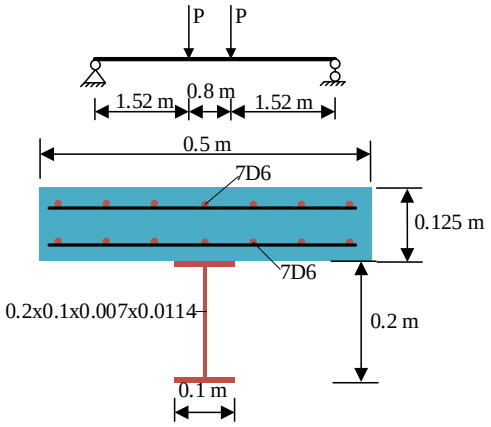

a) Geometry and cross section

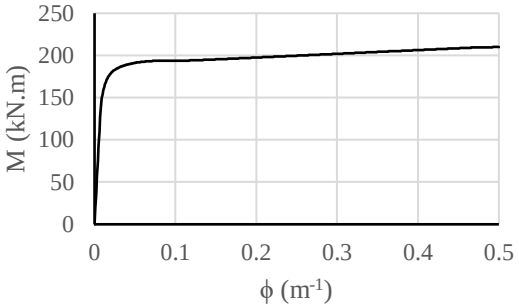

b) Developed moment-curvature curve

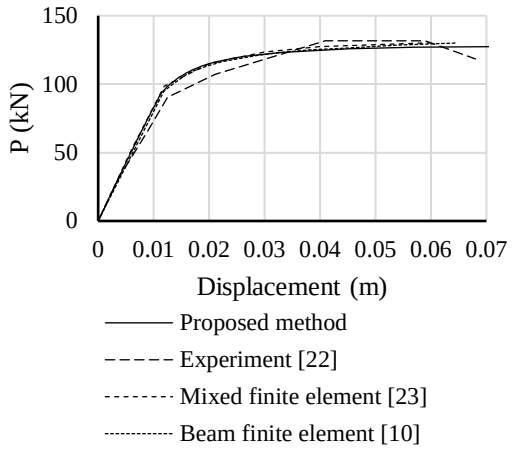

c) Load-displacement curves at mid-span

Fig. 7. The test girder SCB-1 [22,23]

Figure 8c presents the load-displacement curves from the analyses and the test results for the SCB-3 girder. The proposed method and the beam finite element method [10] show excellent agreement with the test results [22], whereas the mixed finite element method [23] overestimates the girder's capacity.

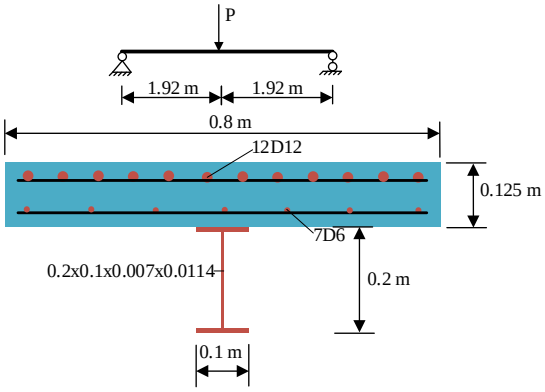

a) Geometry and cross section

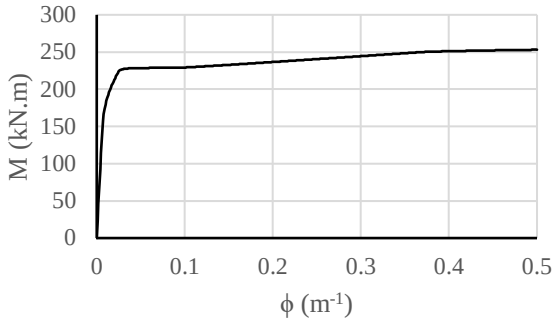

b) Developed moment-curvature curve

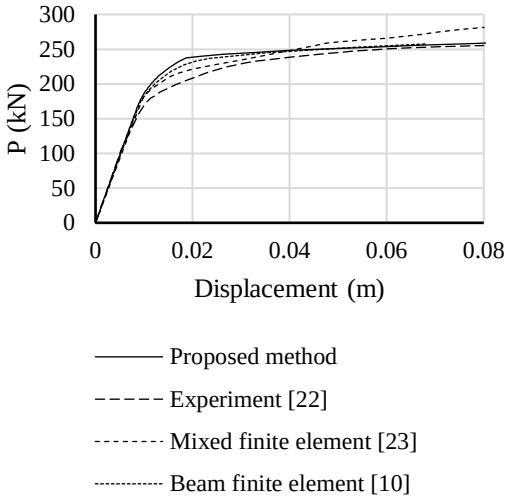

c) Load-displacement curves at mid-span

Fig. 8. The test girder SCB-3 [22,23]

All analyses neglect the shear slip effect between the concrete slab and the steel girder, the load-deflection curves projected by the proposed method and other methods exhibit slightly greater stiffness compared to the test results, particularly immediately after yielding as shown in Figs. 7c and 8c.

The plastic hinge method [4-7,24] was employed for additional analyses to ensure the reliability and high accuracy of the proposed method. In the plastic hinge method, the girders are divided into number of elements and the plastic hinges are assumed to form at the ends of the elements only. The comparisons of the load-displacement curves in Figs. 9a and 9b reveal no discrepancies between the methods. It can be concluded that the proposed method is efficient, straightforward, and highly accurate.

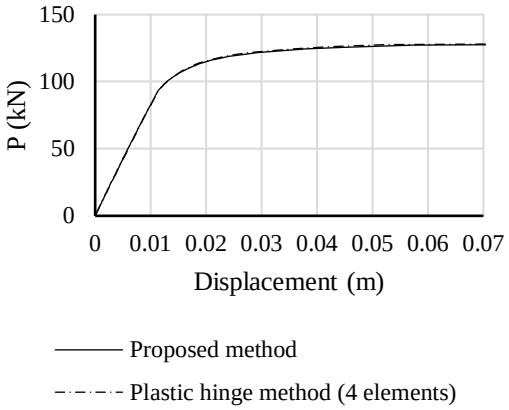

a) SCB-1 girder

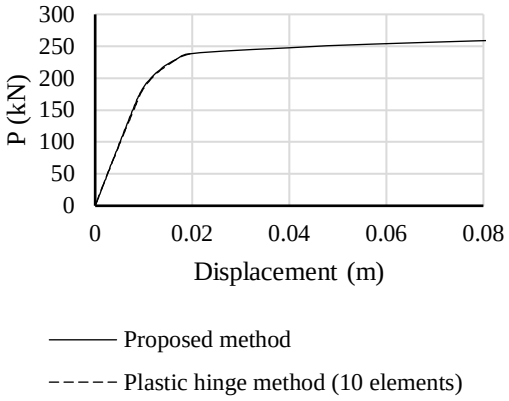

b) SCB-3 girder

Fig. 9. Comparison of the proposed method with the plastic hinge method

5. CONCLUSIONS

This study introduces a novel approach for determining moment-curvature curves and provides an exact analytical solution for the nonlinear behavior of statically determinate steel-concrete composite girders. The following conclusions can be drawn:

- The proposed method achieves higher accuracy compared to the mixed finite element method and the plastic hinge method when the latter uses a single element.
- The analysis results of the proposed method align perfectly with those obtained from beam element and plastic hinge methods that account for gradual and distributed yielding.
- Validation through comparisons with two full-scale test results from the literature, showing either acceptable discrepancies or high accuracy in determining the girder capacities, demonstrates strong consistency and confirms

the robustness of the proposed method.

The proposed method combines simplicity with high accuracy, making it a practical and reliable tool for analyzing statically determinate girders. Additionally, this approach can be extended to analyze reinforced concrete and prestressed reinforced concrete girders, provided the moment-curvature curves for these sections are available. This versatility enhances its utility for both research applications and engineering practice.

6. REFERENCES

[1] AbdElrahman A.M., Hussein M.M. and Attia W.A.L., Modified Web Slenderness Classification for Composite Girders in Code Provisions, International Journal of GEOMATE, 20(80), 2021, pp.168-175.

[2] Al-Haddad S.A., Fattah M.Y., Al-Azawi T.K. and Al-Haddad L.A., Three-dimensional analysis of steel beam-column bolted connections. Open Engineering, 14(1), 2024, pp.1-10.

[3] Eddine W.N., Tarhini K. and Mabsout M., Influence of railing stiffness on single-span two lane steel girder bridges. International Journal of GEOMATE, 19(73), 2020., pp.33-40.

[4] Li G. Q. and Li J. J., Advanced analysis and design of steel frames. John Wiley & Sons, 2007, pp.1-371.

[5] Ngo-Huu C. Practical advanced analysis of steel-concrete composite structures using fiber-hinge method. Ph.D. Dissertation, Department of Civil and Environmental Engineering, the Graduate school of Sejong University, 2006, pp.1-104.

[6] Ngo-Huu C., Kim S. E. and Oh J. R., Nonlinear analysis of steel frames using fiber plastic hinge concept. Engineering Structures, 29, 2007, pp.649-57.

[7] Nguyen P. C. and Kim S. E., Second-order spread-of-plasticity approach for nonlinear time-history analysis of space semi-rigid steel frames. Finite Elements in Analysis and Design, 105, 2015, pp.1-15.

[8] Deng L. and Ghosn M., Nonlinear analysis of composite steel girder bridges. Engineering Journal, 37(4), 2000, pp.140-156.

[9] Jiang X. M., Chen H. and Liew J. Y. R., Spread of plasticity analysis of three-dimensional steel frames. Journal of Constructional Steel Research, 58, 2002, pp.193-212.

[10] Chiorean C. G., A computer method for nonlinear inelastic analysis of 3D composite steel-concrete frame structures. Engineering Structures, 57, 2013, pp.125-152.

[11] Bui V.T., Truong V.H., Trinh M.C. and Kim S.E., Fully nonlinear analysis of steel-concrete composite girder with web local buckling effects. International Journal of Mechanical Sciences, 184, 2020, p.105729.

[12] Ngo-Huu C. and Kim S. E., Practical nonlinear analysis of steel-concrete composite frames using fiber-hinge method. Journal of Constructional Steel Research, 74, 2012, pp.90-97.

[13] Wang Y., Wang Q., Dong J. and Peng Y., Ultimate analysis of steel structures based on fiber hinge model and time-varying structure theory. International Journal of Steel Structures, 15, 2015, pp.567-579.

[14] Ravi Mullapudi T., and Ayoub A., Fiber beam analysis of reinforced concrete members with cyclic constitutive and material laws. International Journal of Concrete Structures and Materials, 12(1), 2018, pp.1-16.

[15] AASHTO/NSBA, Guidelines for Steel Girder Bridge Analysis, 2019, pp.1-214.

[16] Kent D. C. and Park R., Flexural Members with Confined Concrete. Journal of the Structural Division ASCE, 97(ST7), 1971, pp.1969-1990.

[17] ACI Committee, Building code requirements for structural concrete and commentary. In American Concrete Institute, 2008, pp.1-471.

[18] Vebo A. and Ghali A., Moment-Curvature Relations of Reinforced Concrete Slab. J Struct Div ASCE, 103(ST3), 1977, pp.515–531.

[19] Belarbi A. and Hsu T. T., Constitutive laws of concrete in tension and reinforcing bars stiffened by concrete. Structural Journal, 91(4), 1994, pp.465-474.

[20] Hoang N. H., Plastic analysis of concrete-steel frame under static load. Dissertation, Hanoi Architectural University (in Vietnamese), 2020, pp.1-178.

[21] Bear H. S., A primer of Lebesgue integration. Academic Press 2002, pp.1-164.

[22] Nie J. and Cai C. S., Steel-concrete composite beams considering shear slip effects. Journal of Structural Engineering, 129(4), 2003, pp.495-506.

[23] Nie J., Tao M., Cai C. S. and Chen G., Modeling and investigation of elasto-plastic behavior of steel-concrete composite frame systems. Journal of Constructional Steel Research, 67(12), 2011, pp.1973-1984.

[24] Hoang H.N., Vu Q.A. and Nghiem M.H., An Approximation of Yield Surface for Doubly Symmetrical Sections of Steel Structures. Periodica Polytechnica Civil Engineering, 69(1), 2025, pp. 321-332.